The Astrophysical Journal, 739:8 (13pp), 2011 September 20 doi:10.1088/0004-637X/739/1/8

ACCELERATION OF CORONAL MASS EJECTIONS FROM THREE-DIMENSIONAL RECONSTRUCTION OF *STEREO* IMAGES

Anand D. Joshi and Nandita Srivastava
Udaipur Solar Observatory, Physical Research Laboratory, P.O. Box 198, Badi Road, Udaipur 313001, India; janandd@prl.res.in
Received 2011 May 2; accepted 2011 June 16; published 2011 August 29

ABSTRACT

We employ a three-dimensional (3D) reconstruction technique for the first time to study the kinematics of six coronal mass ejections (CMEs), using images obtained from the COR1 and COR2 coronagraphs on board the twin *STEREO* spacecraft, and also the eruptive prominences (EPs) associated with three of them using images from the Extreme UltraViolet Imager. A feature in the EPs and leading edges (LEs) of all the CMEs was identified and tracked in images from the two spacecraft, and a stereoscopic reconstruction technique was used to determine the 3D coordinates of these features. True velocity and acceleration were determined from the temporal evolution of the true height of the CME features. Our study of the kinematics of the CMEs in 3D reveals that the CME LE undergoes maximum acceleration typically below 2 $R_{\odot}$. The acceleration profiles of CMEs associated with flares and prominences exhibit different behaviors. While the CMEs not associated with prominences show a bimodal acceleration profile, those associated with prominences do not. Two of the three associated prominences in the study show a high and increasing value of acceleration up to a distance of almost 4 $R_{\odot}$, but acceleration of the corresponding CME LE does not show the same behavior, suggesting that the two may not be always driven by the same mechanism. One of the CMEs, although associated with a C-class flare, showed unusually high acceleration of over 1500 m s^{-2}. Our results therefore suggest that only the flare-associated CMEs undergo residual acceleration, which indicates that the flux injection theoretical model holds well for the flare-associated CMEs, but a different mechanism should be considered for EP-associated CMEs.

Key words: Sun: coronal mass ejections (CMEs) – Sun: filaments, prominences

1. INTRODUCTION

Coronal mass ejections (CMEs) result from a loss of equilibrium in the magnetic configuration in the solar corona (Priest 1988; Klimchuk 2001). Several factors like, flux emergence, flux cancellation, reconnection, shear, etc., are thought to be responsible for this loss of equilibrium (Forbes et al. 2006; Seaton et al. 2011). Once the equilibrium is lost, the energy needed by the CME for its propagation is derived from the surrounding magnetic field (Forbes 2000; Low 2001). Very often, the energy of the surrounding field is sufficient not only to propel a CME but also to accelerate it (Alexander 2006).

Zhang & Dere (2006) have categorized the evolution of CMEs into a three-phase process involving initiation, acceleration, and propagation (Figure 1 in their paper). According to Zhang & Dere (2006), the initiation phase is the phase of slow rise of CMEs; in the acceleration phase they undergo a very rapid increase in their velocity; while in the propagation phase the CME velocity remains more or less constant, i.e., it experiences almost zero acceleration. Using LASCO (Brueckner et al. 1995) observations on board the *Solar and Heliospheric Observatory* (*SOHO*) spacecraft (Domingo et al. 1995), Yashiro et al. (2004) has observed that the CME velocity in the outer corona varies from less than 100 km s^{-1} to over 3000 km s^{-1}. The propagation of CMEs can be understood if we consider the forces acting on them, which are the Lorentz force, gravitational force, and drag because of the ambient solar wind. Of the three forces, the drag force is the strongest beyond a few solar radii, and the other two can be neglected (Gopalswamy et al. 2001; Cargill 2004; Vršnak et al. 2010). This is further supported by results obtained by Gopalswamy et al. (2000). They have observed that although initial CME speeds range from 124 to 1056 km s^{-1}, the speeds of the corresponding interplanetary ejecta are found to lie in the range of 320–650 km s^{-1}, which is more or less the speed of the ambient solar wind. Cargill (2004) has reported that speeds of interplanetary CMEs (ICMEs) corresponding to CMEs with speeds ranging from 100 to 2000 km s^{-1}, as measured from coronagraphs, lie within 100–200 km s^{-1} of the ambient solar wind. However, the time a CME takes to reach the Earth, the transit time, is known to vary from less than a day to over four days. This indicates that most of the CME dynamics occurs closer to the Sun. Vršnak et al. (2010) have reported that transit times of broad, low-mass CMEs depend mainly on the surrounding solar wind speed, while those of narrow, massive CMEs depend mainly on the initial speeds of the CMEs. Recently, Manoharan & Mujiber Rahman (2011) have also found that most of the ICMEs tend to attain speeds close to that of the ambient solar wind, and have estimated travel times of the CMEs to reach a distance of 1 AU based on the CME initial speed and drag due to solar wind.

CMEs have been classified on the basis of their source regions. Gosling et al. (1976), using the coronagraph on the *Skylab* spacecraft, were the first ones to report that CMEs associated with flares are faster than those associated with prominences. This was supported by observations of CMEs by MacQueen & Fisher (1983) who used the *K*-coronameter at Mauna Loa Solar Observatory. In addition, they also observed that the former type showed lower acceleration with an increase in height than the latter. Sheeley et al. (1999) have also reported a similar result based on their technique to track features observed in *SOHO*/LASCO coronagraphs. Moon et al. (2002) in a statistical study involving over 3200 CMEs observed from *SOHO*/LASCO have reported that flare-associated CMEs have a higher median speed than those associated with eruptive prominences (EPs). Their study also found that although the median acceleration of all the events is zero, it decreases a little for CMEs with high speeds

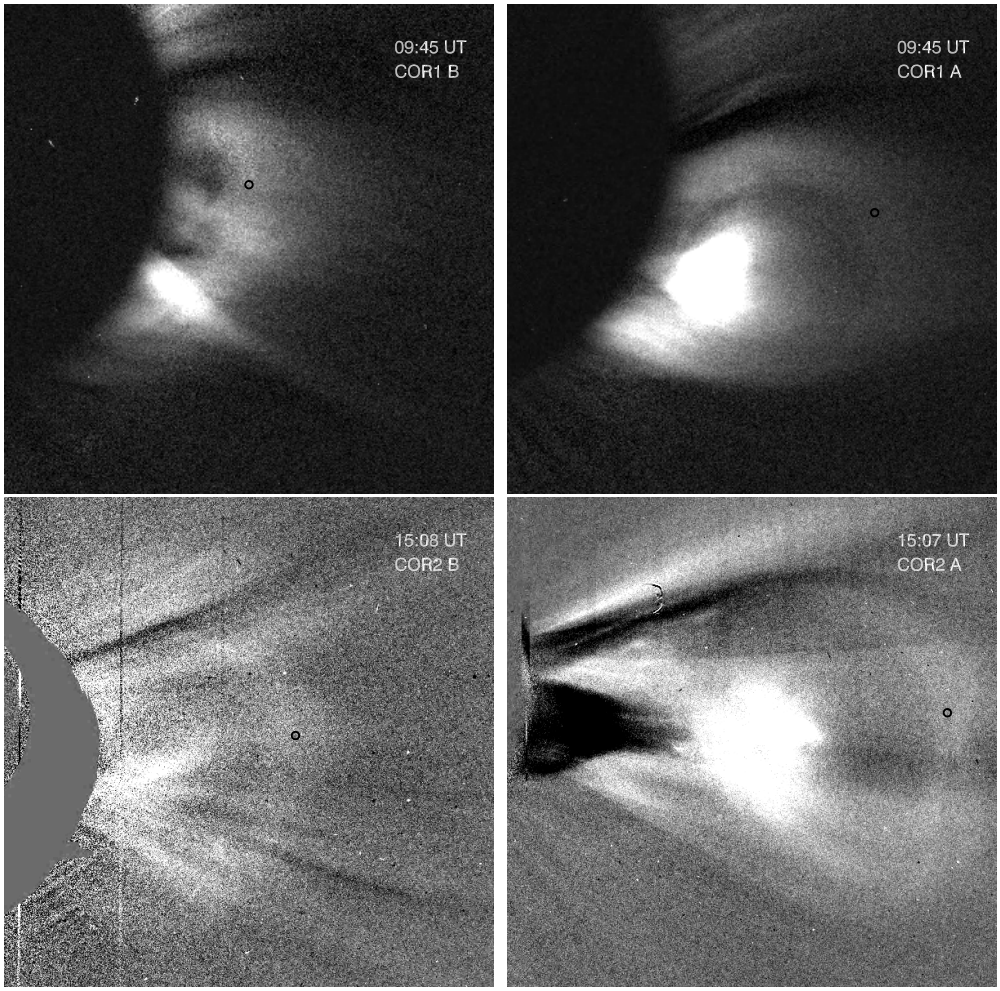

Figure 1. Images of the CME on 2007 November 16 seen in images from COR1 (top panels) and COR2 (bottom panels), as seen from *STEREO B* (left) and *A* (right).

($>500\,\mathrm{km\,s^{-1}}$). Srivastava et al. (1999, 2000) have found that gradual CMEs attain the speed of the ambient solar wind at about 20 $R_\odot$ from the Sun. Results from Gopalswamy et al. (2001) are also consistent with this study, who reported deceleration as high as $-100\,\mathrm{m\,s^{-2}}$ for fast CMEs (speed $>900\,\mathrm{km\,s^{-1}}$) from a combined study of *SOHO*/LASCO and radio observations from the *Wind* spacecraft.

Chen & Krall (2003) have studied the acceleration of three CMEs using *SOHO*/LASCO observations and proposed that CME acceleration occurs in two phases, the "main" phase and the "residual" phase. While most of the acceleration occurs in the main phase, there lies a second phase of acceleration known as the residual acceleration in the outer corona. Chen & Krall (2003) and Chen et al. (2006) have identified the main acceleration phase as the interval over which the Lorentz force is the most dominant, while during the residual phase, the Lorentz force is comparable to the two other forces, viz, gravity and drag. They have employed the magnetic flux rope model (Chen 1989) to show a relation between the height at the peak of main acceleration phase and the footpoint separation of the CME flux rope. In their model, Chen & Krall (2003) have proposed that a change in the duration of the flux injection (Krall et al. 2000) determines the strength of the residual acceleration phase. Similarly, Zhang & Dere (2006) have also reported two such phases of acceleration based on their study of 50 CMEs observed from *SOHO*/LASCO.

All the studies cited above use a single viewpoint to observe the CMEs. The results then inherently suffer from projection effects of the transients onto the plane of the sky. In order to overcome this, we decided to look at CMEs from the stereoscopic vision of the *Solar TErrestrial RElations Observatory* (*STEREO*; Kaiser et al. 2008). The *STEREO* spacecraft provide two viewpoints of the prominences and the associated CMEs. We have used a stereoscopic reconstruction technique to determine the true physical coordinates of a solar feature (Joshi & Srivastava 2011). The stereoscopic reconstruction would allow us to observe the evolution of the true height of prominences and CMEs, and hence their true velocity and acceleration. From this we can examine if the acceleration truly exhibits a bimodal profile as the model suggests. This will also give us a clue about the initiation and propagation of CMEs in the corona.

2. DATA AND OBSERVATIONS

The Sun Earth Connection Coronal and Heliospheric Investigation (SECCHI; Howard et al. 2008) suite of instruments on the *STEREO* spacecraft carries two white-light coronagraphs, COR1 and COR2, with fields of view (FOVs) 1.4–4.0 $R_\odot$ and 2.0–15.0 $R_\odot$, respectively, and the Extreme UltraViolet Imager (EUVI) imaging the Sun at four wavelengths in the extreme ultraviolet band. We have used images obtained from the two coronagraphs to study six CMEs that occurred on 2007

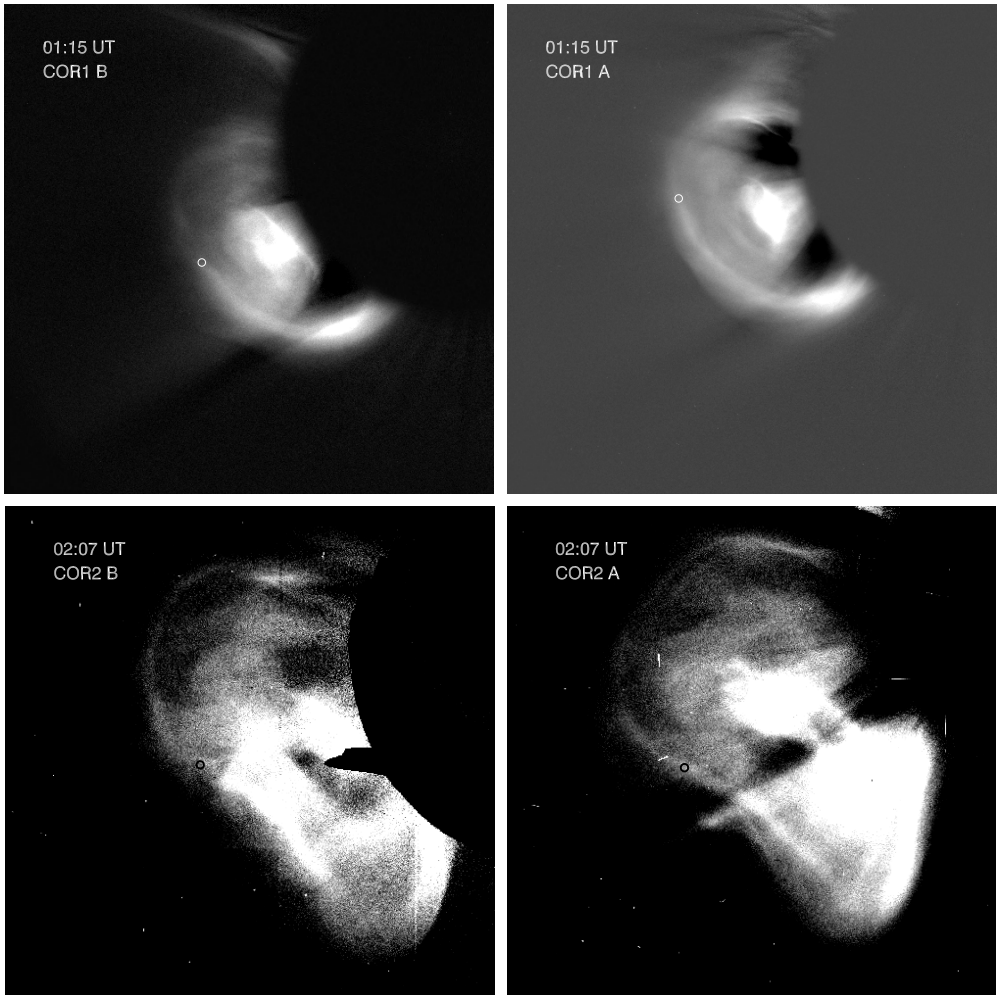

Figure 2. Images of the CME on 2007 December 31 seen, similar to Figure 1.

November 16, 2007 December 31, 2008 April 9, 2009 December 16, 2010 April 13, and 2010 August 1. The cadence of images for the cases analyzed was at best 5 minutes for COR1 and 15 minutes for COR2. In addition, three EPs that were associated with the CMEs on 2008 April 9, 2010 April 13, and 2010 August 1 were also analyzed using 304 Å images from the EUVI instrument having a cadence of 10 minutes. A sample image of each event observed from coronagraphs COR1 and COR2, and EUVI 304 Å for the three EPs, are shown in Figures 1–6. The soft X-ray flux data from *Geostationary Operational Environmental Satellite* (*GOES*) was used to determine the start and peak times of the flare associated with the CMEs on 2007 December 31 and 2009 December 16.

A feature that could be identified and tracked in all the simultaneous pairs of images from the spacecraft was used for stereoscopic reconstruction. To be able to unambiguously identify the feature in FOVs of both the *STEREO* coronagraphs, we had to select a feature in the inner part of the LE, and not the outermost feature in the LE. The reconstruction technique involves rotating the heliocentric Earth ecliptic coordinate system separately for *STEREO Ahead* (*A*) and *Behind* (*B*) so that one of the axes of the coordinate system lies along the Sun–spacecraft line. As a result, the plane perpendicular to this axis becomes the image plane for the concerned spacecraft, and the image coordinates of the feature to be reconstructed are the projection of the feature in this rotated coordinate system for that spacecraft (Joshi & Srivastava 2011). Using rotation matrices, and applying the epipolar constraint, it is then possible to obtain the true coordinates of the feature in the heliographic coordinate system.

2.1. Analysis

We have used the stereoscopic reconstruction technique as described in Joshi & Srivastava (2011) to obtain the true coordinates for a feature in the leading edge (LE) of all the CMEs, and the associated EPs in three of the events, in the heliographic coordinate system. The reconstruction technique can be used for on-disk EUVI images, as well as coronagraph images from COR1 and COR2. The errors in determination of the height from EUVI, COR1, and COR2 are 0.02 $R_\odot$, 0.12 $R_\odot$, and 0.6 $R_\odot$, respectively. On fitting a polynomial function to the true height, and taking its first and second derivatives, we determine the true speed and acceleration of the EP and the LE. Since we are interested in looking at CME acceleration profiles, we only present the relevant results and not all the information that we derive from the reconstruction, namely, the Stonyhurst latitudes and longitudes. In Figures 7–12, we have shown the evolution of true height, velocity, and acceleration with time. However, to know the exact height at which acceleration of the CME occurred, we have plotted the speed and acceleration as a function of the true height of the tracked feature. We

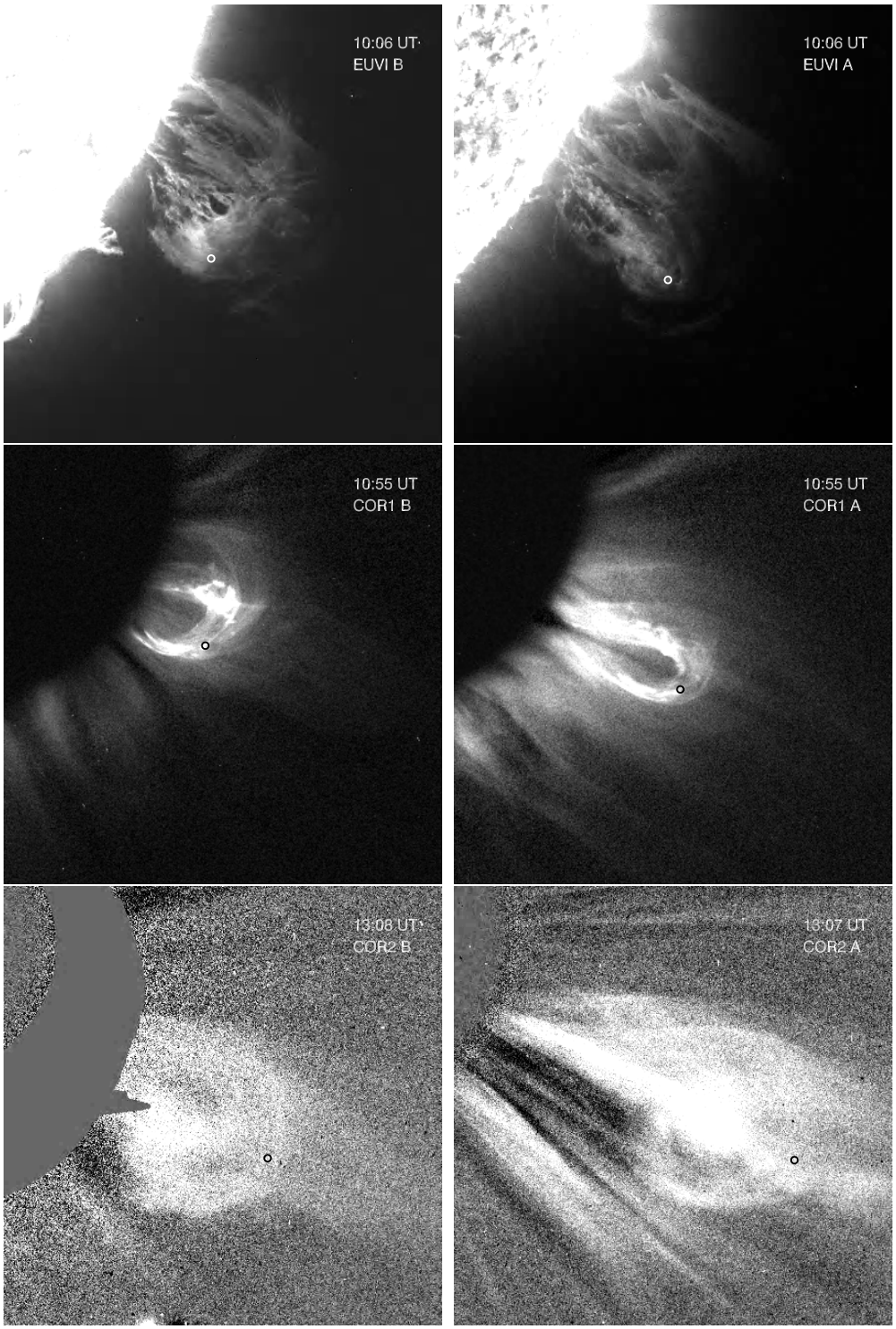

Figure 3. Images of the EP and associated CME on 2008 April 9 seen in images from EUVI 304 Å (top panels), COR1 (middle panels), and COR2 (bottom panels), as seen from *STEREO B* (left) and *A* (right).

have marked the reconstructed points obtained from COR1 coronagraph with plus signs, and those from COR2 with asterisks, while triangles are used to indicate features observed in EUVI 304 Å images, wherever applicable. The polynomial functions used to fit the heights of the events are further used to determine errors in velocity and acceleration. The errors in heights are used in the error propagation formula, and the maximum errors in velocity and acceleration are found to be 40 km s^{-1} and 25 m s^{-2}, respectively.

3. RESULTS AND DISCUSSION

3.1. 2007 November 16 CME

Both *STEREO* spacecraft observed this event as a faint and slow CME on the southwest limb of the Sun (Figure 1). The CME first appeared in the COR1 A FOV at 07:25 UT, and in the COR1 B FOV at 08:15 UT. The CME entered the COR2 A FOV at 10:37 UT, and in the COR2 B FOV 2 hr later at 12:37 UT. EUVI A 304 Å images show a surge eruption on the far side of

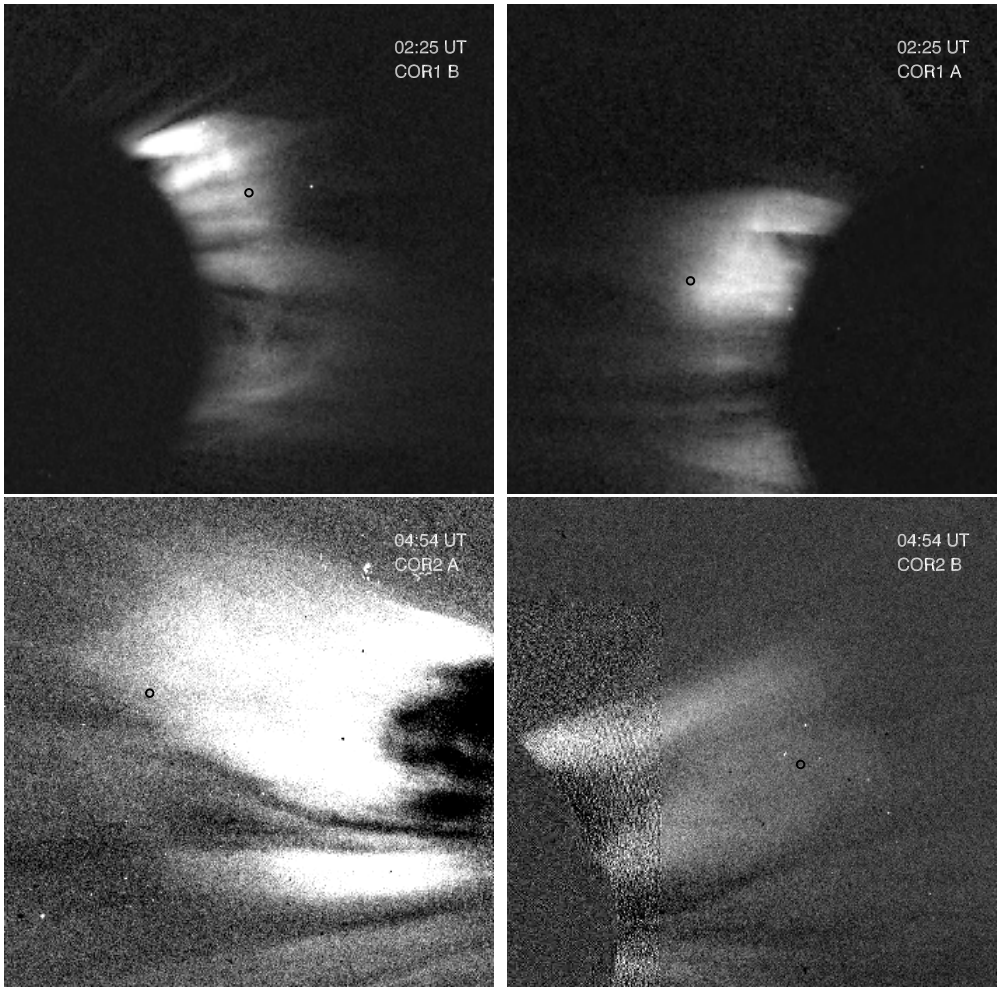

Figure 4. Images of the CME on 2009 December 16 seen, similar to Figure 1.

the Sun. The surge eruption commenced at 06:26 UT and could be observed up to 09:46 UT.

Figure 7 shows results of the stereoscopic reconstruction technique applied to a feature on the LE of this CME. The plots on the left in Figure 7 show the change in height, and the resultant speed and acceleration obtained from derivatives of a polynomial function fitted to the true height, as a function of time. The plots on the right show speed and acceleration as a function of true height. From this figure we find that the CME speed increases very rapidly in the COR1 FOV, and is almost constant in the COR2 FOV. The acceleration of the CME in the COR1 FOV is $50\,\mathrm{m\,s^{-2}}$, but it falls rapidly, and is down to $11\,\mathrm{m\,s^{-2}}$ at about $3.7\,R_{\odot}$. Thus, the maximum value of acceleration and the height at which the CME attained this value are not available to us. We however point out that the maximum acceleration of the CME occurred at or less than $2\,R_{\odot}$ in height. In the higher corona, i.e., in the COR2 FOV, we see that the acceleration once again rises by a small amount to reach $18\,\mathrm{m\,s^{-2}}$ at a height of around $8\,R_{\odot}$, which can be attributed to the residual acceleration phase consistent with the model proposed by Chen & Krall (2003).

3.2. 2007 December 31 CME

This was a bright CME with a well-defined symmetrical LE on the southeast limb of the Sun, as seen in Figure 2. The CME was associated with a C8-class flare which originated in NOAA active region (AR) 10980. The CME appeared in the COR1 B FOV at 00:55 UT, and at 01:00 UT in the COR1 A FOV. The CME crossed the COR1 FOV in about 1 hr, indicating that it was a relatively fast CME, and appeared in the COR2 FOV at 01:37 UT in both spacecraft. This CME showed an unusual cusp in its LE, which was distinctly visible in the COR2 images. Thernisien et al. (2009) have used the graduated cylindrical shell model (Thernisien et al. 2006) to fit two shells flanking the cusp for this CME, and employed the forward modeling technique to determine the true direction of its propagation and speed. We have used this feature for the purpose of reconstruction. On the eastern limb of the 304 Å image from EUVI B, a flare can be seen at 00:46 UT, followed by opening up of the field lines which can be clearly seen in the 171 Å and 195 Å images from EUVI B. From the *GOES* soft X-ray flux data, we find that the flare started at 00:45 UT and peaked at 01:03 UT.

The CME speed increased in the lower corona to reach $812\,\mathrm{km\,s^{-1}}$ at a height of $2.8\,R_{\odot}$ and showed a little dip before attaining a constant value of around $870\,\mathrm{km\,s^{-1}}$ (Figure 8). This CME has the highest value of maximum acceleration of all the CMEs studied here, which is over $1500\,\mathrm{m\,s^{-2}}$ at a height of about $2\,R_{\odot}$. Such a high value is observed for CMEs associated with flares, which are termed as impulsive by Sheeley et al. (1999) and Moon et al. (2002). However, the flare in this case was classified as X-ray class C8, and such high values of CME

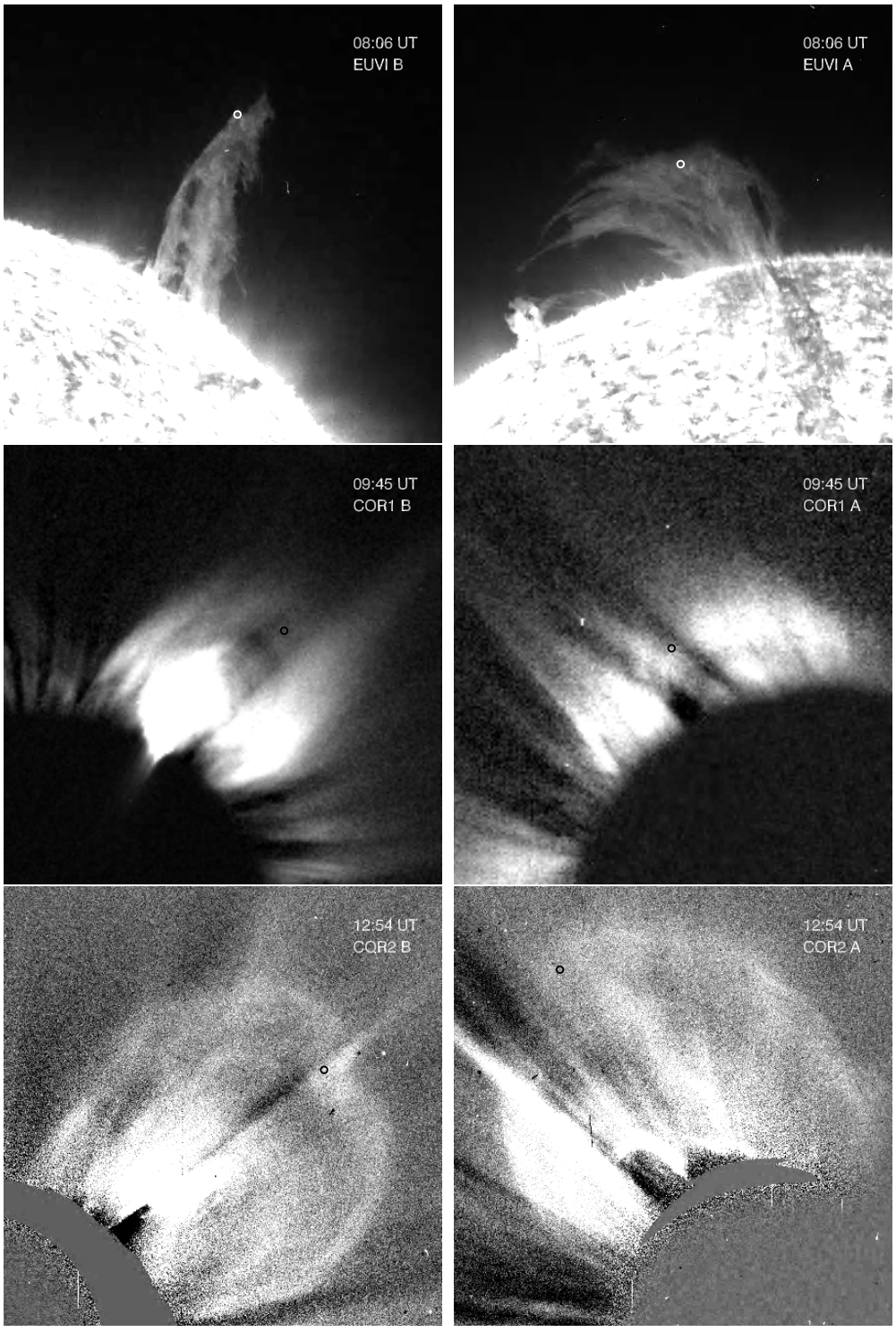

Figure 5. Images of the EP and the associated CME on 2010 April 13, similar to Figure 3.

acceleration are earlier reported to be associated with X-class flares. Such a high value of acceleration has also been reported by Alexander et al. (2002) for a CME associated with an X1.2-class flare. Also, assuming that this CME achieved its maximum value somewhere below 2 $R_{\odot}$, we note that this favors the CME model proposed by Chen & Krall (2003), where they predict a bimodal acceleration profile. This CME has previously been analyzed by several researchers. Among them, Temmer et al. (2010) have found acceleration of this CME to be 1300 m s^{-2}, while Lin et al. (2010) have found it to be over 1000 m s^{-2}; both results were obtained from stereoscopic reconstruction of the CME. The large difference in acceleration values between our results and those cited above can be attributed to the different assumptions involved in the numerous reconstruction techniques (Mierla et al. 2010).

3.3. 2008 April 9 CME and EP

The CME on 2008 April 9 was associated with an AR prominence, and was observed on the southwest solar limb,

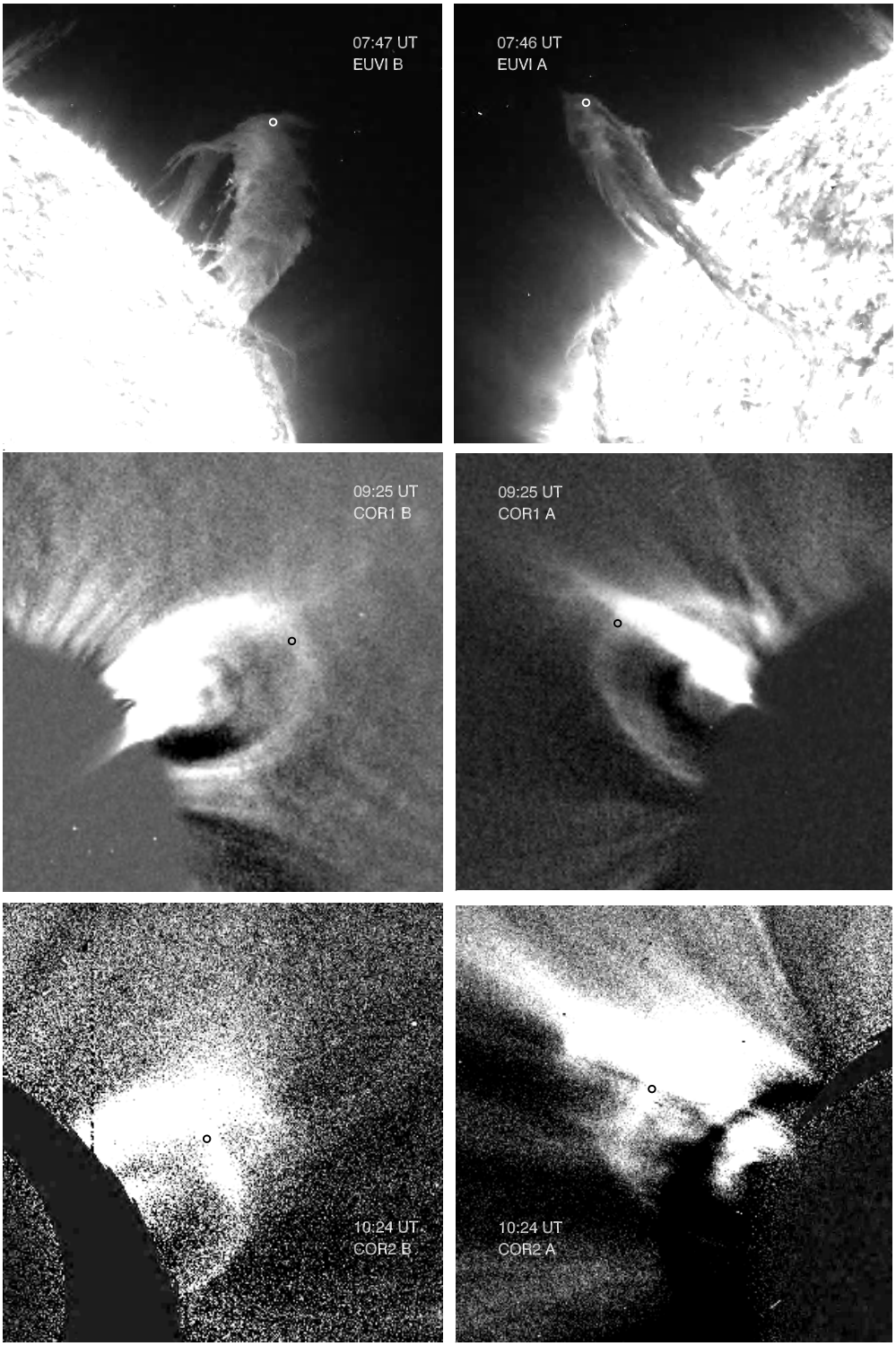

Figure 6. Images of the EP and the associated CME on 2010 August 1, similar to Figure 3.

as shown in Figure 3. The CME first appeared in the COR1 A and B FOVs at 10:15 UT and 10:25 UT, respectively, while it could be just seen in the COR2 A and B FOVs at 12:07 UT. The LE showed a bright knot close to its highest point, which was tracked during the reconstruction. The prominence material could be seen in the 304 Å images from 09:26 onwards in EUVI A and 09:46 UT onwards in EUVI B.

This CME LE showed very smooth changes in both its speed and acceleration, as can be seen from Figure 9. The speed increased until the CME reached about 4 $R_{\odot}$, but the peak of the acceleration profile could not be observed, which, as in previous cases, occurred at a height less than 2 $R_{\odot}$. The acceleration kept on decreasing until it reached a value of around $-14\,\mathrm{m\,s^{-2}}$. Correspondingly, the maximum speed was $530\,\mathrm{km\,s^{-1}}$, and it decreased till the time the LE reached a height of $\sim$11.5 $R_{\odot}$. The prominence associated with this CME showed an increase in acceleration up to a height of almost 4 $R_{\odot}$, until the time it could be observed in the COR1 images. However, the velocity

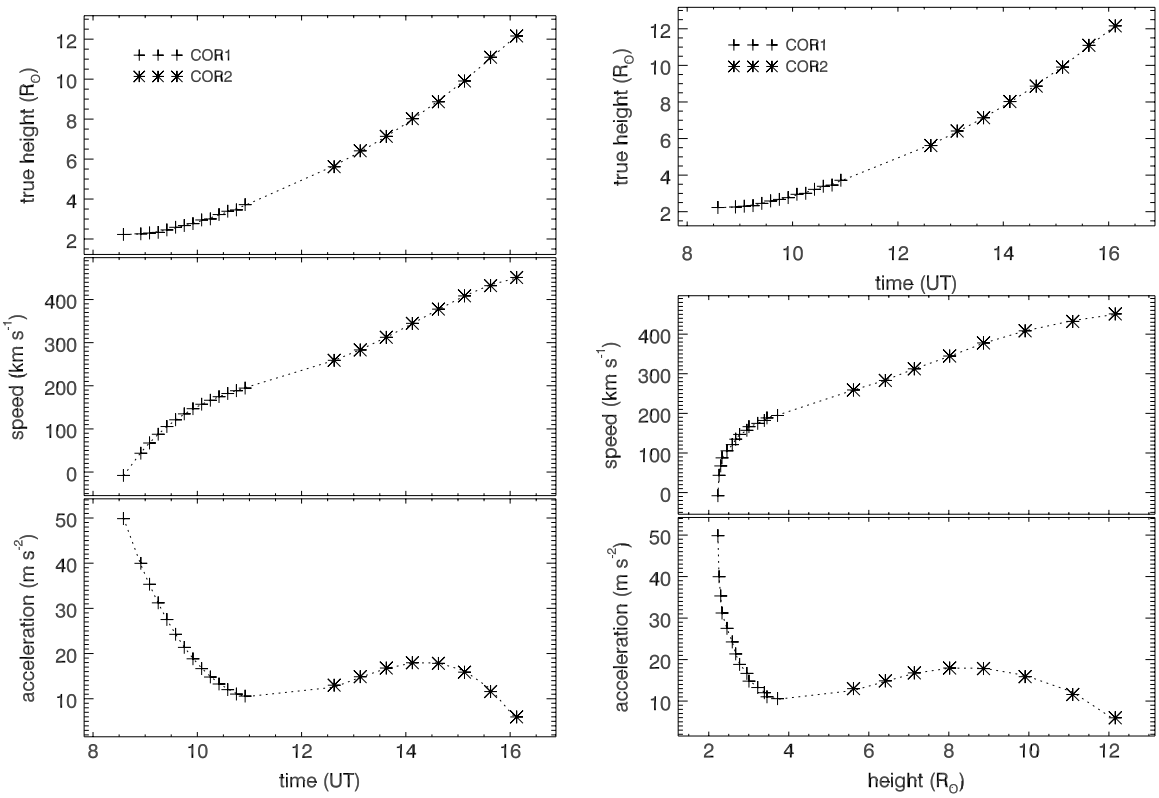

Figure 7. Results from the stereoscopic reconstruction applied to a feature in LE of the CME on 2007 November 16. Left: true height of the CME feature against time in the top panel, followed by the true speed and acceleration against time in the middle and bottom panels, respectively. Right: true height of the CME against time at the top, followed by the true speed and acceleration against true height in the middle and bottom panels, respectively. Plus signs (+) and asterisks (*) indicate that the feature was observed in the COR1 and COR2 FOVs, respectively.

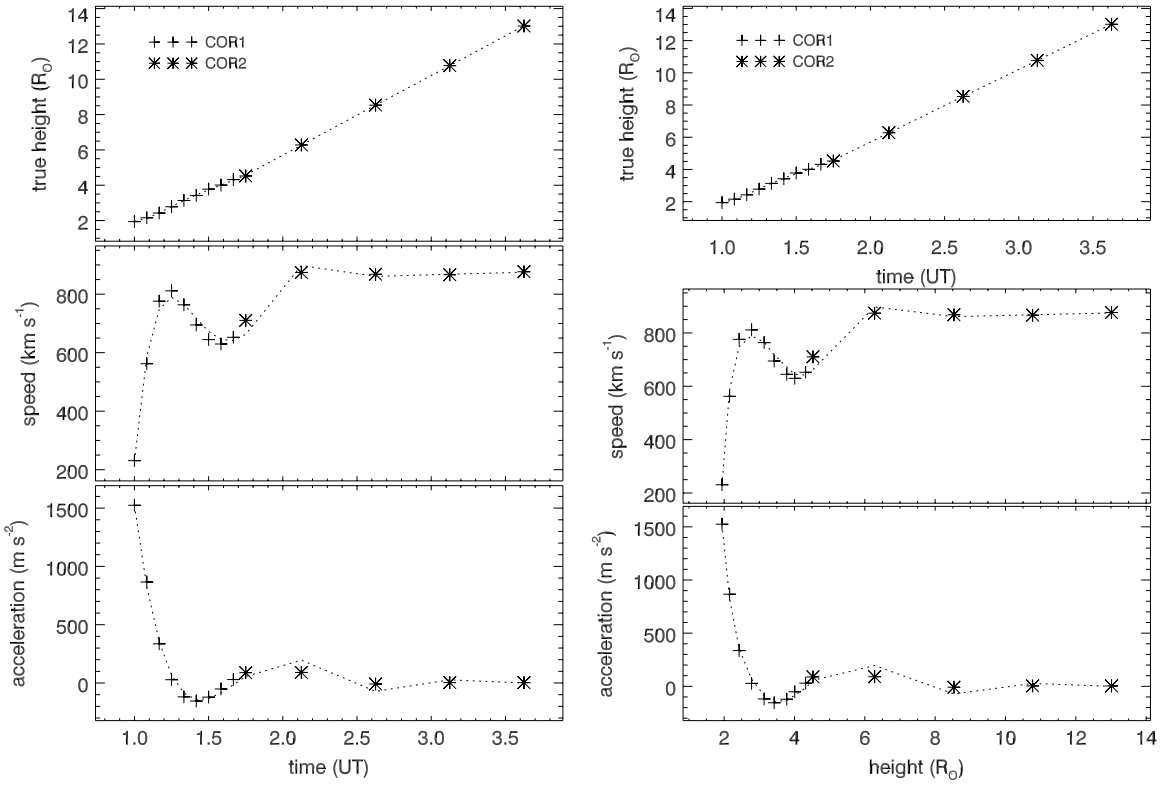

Figure 8. Results from stereoscopic reconstruction of the CME on 2007 December 31, similar to Figure 7.

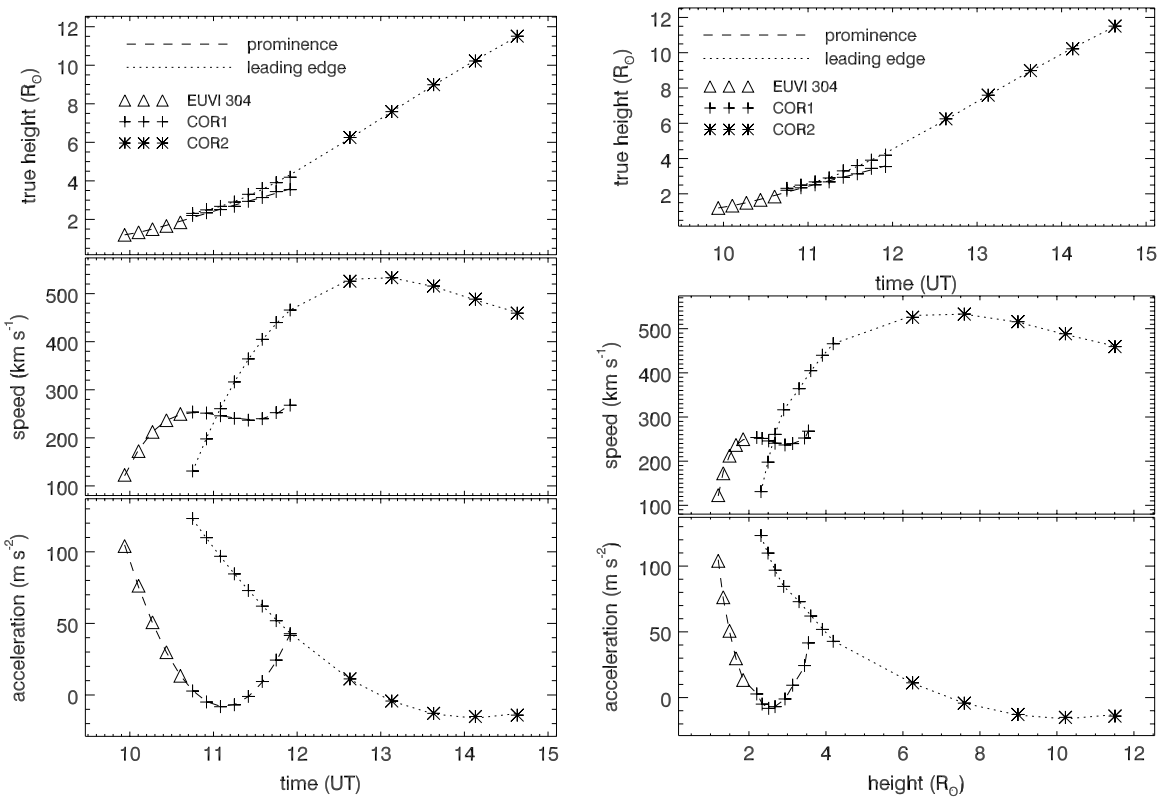

Figure 9. Results from stereoscopic reconstruction of the CME on 2008 April 9, similar to Figure 7. Here, triangles (△) indicate feature observed in EUVI FOV.

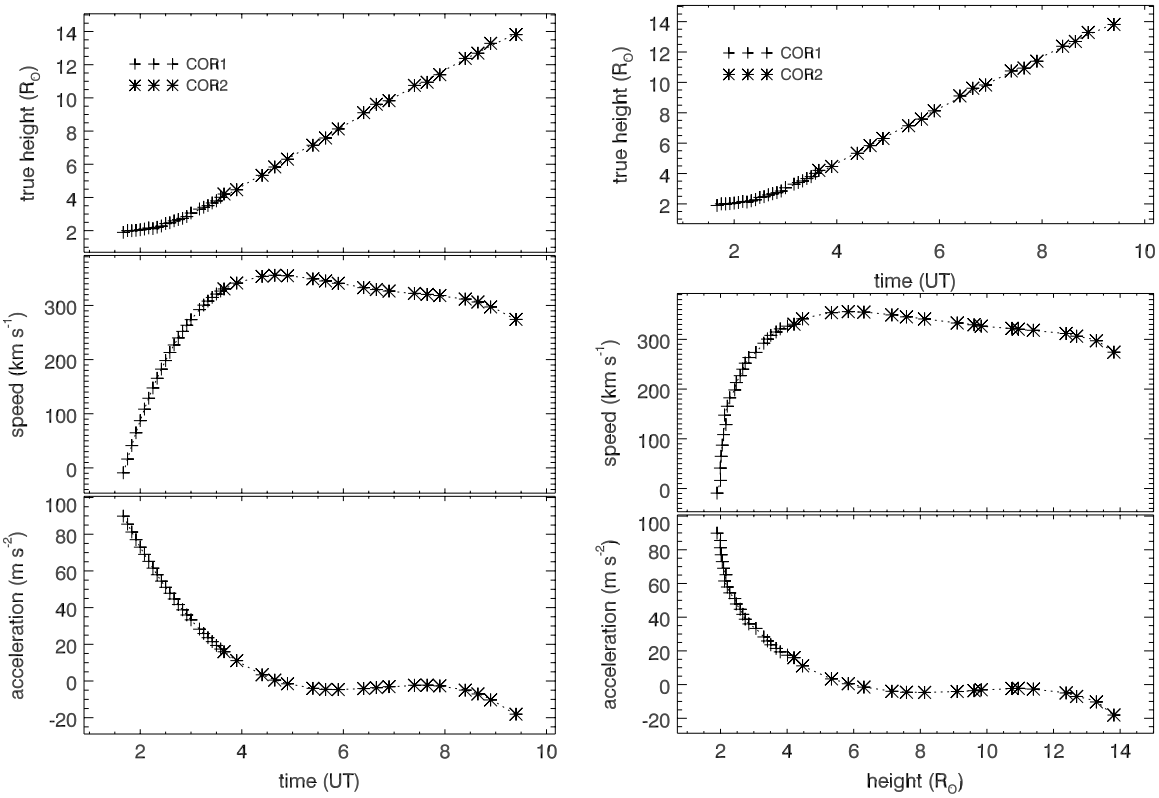

Figure 10. Results from stereoscopic reconstruction of the CME on 2009 December 16, similar to Figure 7.

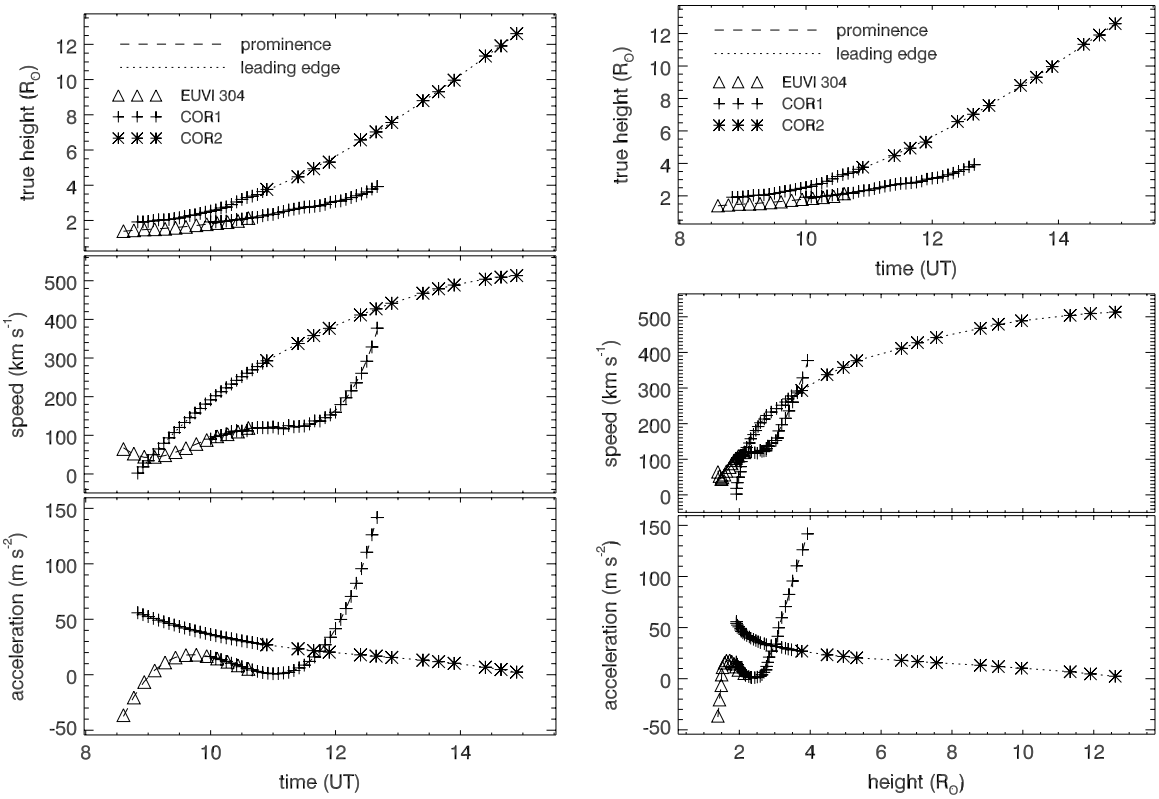

Figure 11. Results from stereoscopic reconstruction of the CME on 2010 April 13, similar to Figure 9.

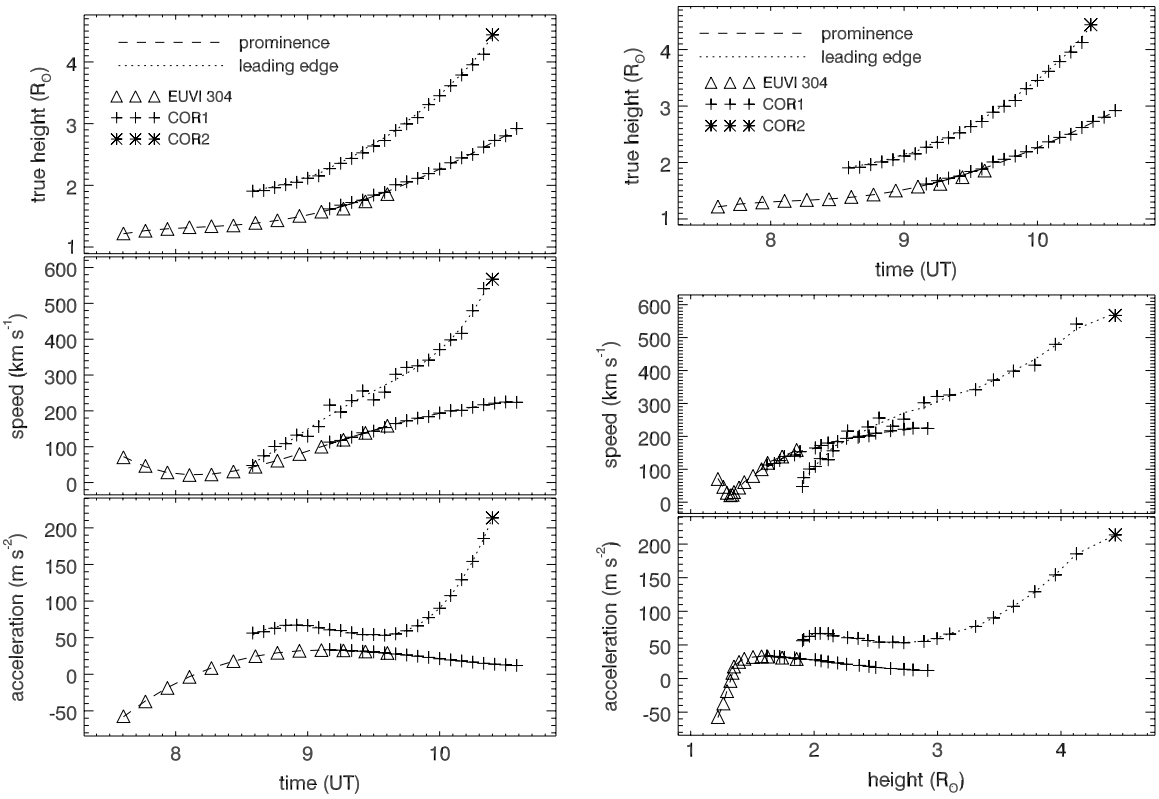

Figure 12. Results from stereoscopic reconstruction of the CME on 2010 August 1, similar to Figure 9.

of the prominence ($\sim$250 km s^{-1}) was found to be less than that of the CME (>400 km s^{-1}).

3.4. 2009 December 16 CME

This CME was associated with a C5.3-class flare in NOAA AR 11035 that started at 00:59 UT, and had its peak at 01:09 UT. The CME first appeared in the COR1 A and B FOVs at 01:40 UT and 01:35 UT, respectively, while it could be just seen in COR2 A and B FOVs at 03:08 UT and 03:39 UT, respectively (Figure 4).

From the COR1 observations, we could not see the peak of the acceleration of the CME LE; we could only observe the acceleration decrease from around 90 m s^{-2} to 0 m s^{-2} as the CME travels from a height of 2 $R_\odot$ to 6 $R_\odot$, as seen in Figure 10. At this height, the CME velocity attains a value of 350 km s^{-1}. Later, at a height of around 11 $R_\odot$, we find that the acceleration has a smaller rise before reaching a value of -20 m s^{-2} at 14 $R_\odot$.

3.5. 2010 April 13 CME and EP

This CME was associated with a large northern polar crown filament, as seen in Figure 5. The filament appeared edge-on on the western limb in the EUVI B FOV, but it could be seen extending from the central meridian right up to the northeast limb in EUVI A. The prominence eruption commenced at 08:36 UT, and the CME LE could be seen at 08:50 and 08:40 UT, respectively, in the COR1 A and B FOVs. The CME LE could be seen in the COR2 FOV at 10:39 UT. The prominence material could also be very conspicuously seen in the images from both the coronagraphs on the two spacecraft.

This CME showed changes in speed and acceleration similar to the CME on 2007 November 16 (Figures 11 and 7). Its speed very rapidly reached a value of 300 km s^{-1} at a height of 3.8 $R_\odot$, and during the same time its acceleration dropped from 60 m s^{-2} to 27 m s^{-2}. The peak of the acceleration however could not be observed. Like the event of 2008 April 9, here too we find the prominence showing an increasing acceleration at least until 4 $R_\odot$.

3.6. 2010 August 1 CME and EP

This CME was also associated with a northern polar crown filament, as seen in Figure 6. The filament appeared as a hedgerow prominence in EUVI B 304 Å images, while the line of sight was along the spine in EUVI A images. The CME was first seen in the COR1 A FOV at 08:10 UT, and at 08:25 UT in the COR1 B FOV. Due to a data gap in the COR2 observations, the CME was seen only in a single image at 10:24 UT in COR2 A and B.

This CME behaved very differently from the others analyzed in this study. Its speed was very low at the start, and it gradually reached the maximum speed of 567 km s^{-1}, at a height of $\sim$4.5 $R_\odot$. At this height, the CME was still accelerating, but owing to a data gap in the COR2 observations, its peak value could not be determined. The maximum acceleration of the prominence was 40 m s^{-2} at a height of about 1.5 $R_\odot$, and then showed a steady decrease to around 10 m s^{-2} at a height of 3 $R_\odot$. The CME LE accelerated very late into its eruption. At a height of 4 $R_\odot$, the LE showed an acceleration value of over 200 m s^{-2}.

4. SUMMARY AND CONCLUSIONS

We have analyzed six CMEs from the coronagraphs COR1 and COR2, and the associated EPs in three of the cases from EUVI on board the identical *STEREO A* and *B* spacecraft. We identified and tracked a feature in the LE of all the CMEs in both COR1 and COR2, and in the associated prominences, wherever applicable. While most of the earlier studies on CME acceleration were carried out using projected measurements, we have used a stereoscopic reconstruction technique (Joshi & Srivastava 2011) to obtain the true coordinates, and hence the true speed and acceleration of the feature. On fitting a polynomial function to the true height, the speed and acceleration of the CMEs as a function of time and true height were determined. The results of the kinematic study of EPs and the CME LEs are shown in Figures 7–12. We summarize the results obtained from the reconstruction in Table 1.

Table 1
Summary of the Six LEs and Three EPs Analyzed Using Three-dimensional Reconstruction

Event	v_{max} (km s^{-1})	Height of v_{max} ($R_\odot$)	a_{max} (m s^{-2})	Height of a_{max} ($R_\odot$)	v at 10 $R_\odot$	a at 10 $R_\odot$
2007 Nov 16 LE	451	12.2	50	2.2	408	16
2007 Dec 31 LE	876	13.0	1524	1.9	860	2
2008 Apr 9 LE	533	7.6	123	2.3	488	−15
2009 Dec 16 LE	356	5.8	90	1.9	488	−15
2010 Apr 13 LE	522	12.6	61	1.9	193	36
2010 Aug 1 LE	567	4.4	213	4.4	...	...
2008 Apr 9 EP	268	3.5	104	1.2	...	...
2010 Apr 13 EP	377	3.9	141	3.9	...	...
2010 Aug 1 EP	224	2.9	34	1.6	...	...

Notes. v_{max} and a_{max} denote the maximum speed and acceleration of the CME calculated. The heights at which CMEs attained these values are also provided. The last two columns show the speed and acceleration of the CMEs at a distance of 10 $R_\odot$.

It is believed that most of the CME acceleration typically occurs in the lower corona. Chen & Krall (2003) have found the height of maximum acceleration of CME to be 2–3 $R_\odot$ from a study of several CMEs; Vršnak (2001) have considered this height to be 4 $R_\odot$. However, from our reconstructed results (Figures 7–12), we observe that in all the cases studied here, the peak of the main phase of acceleration lies below the true height of 2 $R_\odot$. This indicates that most of the CME dynamics occurs closer to the Sun than previously believed, as shown by Chen et al. (2006) from a comparison of observations and models.

Earlier studies (Zhang et al. 2001; Chen & Krall 2003) have observed CMEs in all the three *SOHO*/LASCO coronagraphs which together cover a range from 1.1 to 32 $R_\odot$. In such studies, the initiation phase of the CME as well as the peak of their acceleration could be observed. The COR1 and COR2 coronagraphs together image the solar corona from 1.4 to 15.0 $R_\odot$; however, these are only the plane-of-sky FOVs of the coronagraphs. The minimum value of the true height of the reconstructed features of the corona is approximately 2.0 $R_\odot$. Thus, in most of the cases we do not capture the rise phase acceleration of the LE of CME. In all but one case studied here, the acceleration peak has already passed before we started observing the CME. At this point, it is necessary to point out that the heights determined in this study are true heliocentric distances, hence they are seen to be significantly different than the heights obtained from previous studies, which relied upon observations from a single spacecraft.

The CME on 2007 December 31 was associated with a flare having X-ray class C8; however, it still showed a very high value of acceleration of over 1500 m s^{-2}. Earlier studies have

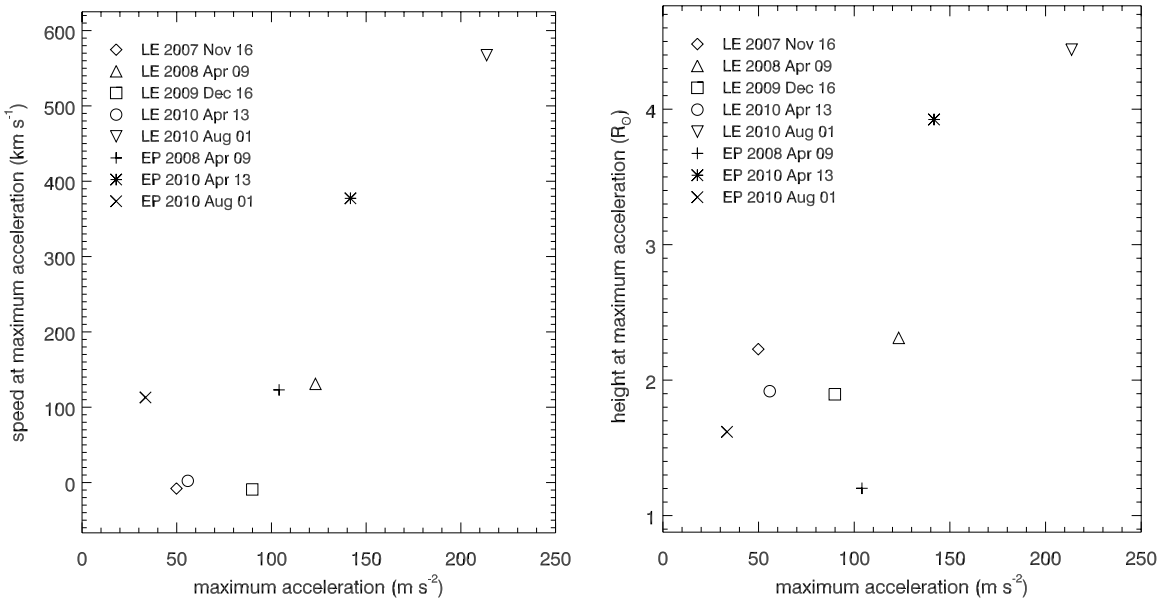

Figure 13. Two scatter plots showing speed (left panel) and height (right panel) at the instance of maximum acceleration and the maximum acceleration itself of the six CMEs and three EPs studied. The legend shows data points corresponding to each event. Data point for the 2007 December 31 CME is not shown since it has a very high value of maximum acceleration.

shown that the acceleration phase of CMEs coincides with the increase in soft X-ray flux due to the associated flare (Neupert et al. 2001; Shanmugaraju et al. 2003). Maričić et al. (2007) have also shown that both the velocity and acceleration of the CME show a significant correlation with the X-ray class of the associated flare. As per the least squares fit obtained from their study, acceleration of the CME associated with a C8 flare should be around 300 m s^{-2}. The value calculated by us, however, is five times more, suggesting that the flare energy alone might not be the only one to drive the CMEs. In such a scenario, the supposition that impulsive and gradual CMEs are respectively associated with flares and EPs (MacQueen & Fisher 1983; Moon et al. 2002) should also be subjected to further scrutiny. Also, deviations to the findings reported by Maričić et al. (2007), where acceleration of CMEs is correlated with the X-ray class of the associated flare, should not be ignored. Raftery et al. (2010) have used soft and hard X-ray observations in addition to *STEREO* observations (Lin et al. 2010) to analyze the 2007 December 31 CME, and have found that it follows the tether-cutting reconnection model.

The results obtained from reconstruction were used to determine maximum acceleration, average acceleration, acceleration magnitude, and acceleration duration, attained by the CMEs and EPs. The time interval between the maximum and the zero value of acceleration is termed as the acceleration duration, while the velocity increase during this time divided by the acceleration duration is termed as the acceleration magnitude (Zhang & Dere 2006). The very high value of acceleration for the 2007 December 31 CME makes the event an "outlier," hence, we have not included that value in the scatter plots in Figure 13. The left panel shows the speed at maximum acceleration plotted against the maximum acceleration. From this figure, we find that in the events we studied, the higher the maximum value of acceleration, the higher is the speed at that instant. While the right panel of Figure 13 shows scatter plot of maximum acceleration and height at the instance of maximum acceleration. This scatter plot suggests that the higher the acceleration, the higher up in the corona it occurs.

Although the acceleration in this study is determined up to the COR2 FOV, it may not be the value with which the CME is traveling at larger distances from the Sun. Based on interplanetary measurements, it was shown earlier by Gopalswamy et al. (2000) that slow CMEs tend to accelerate, while faster ones tend to decelerate. Recently, Davis et al. (2010) have measured the speeds of 26 CMEs from the Heliospheric Imagers (HI), which are part of the SECCHI suite on the *STEREO* spacecraft. In their study, they have found that CMEs with speeds less than 400 km s^{-1} in the COR2 FOV have higher speeds in the HI FOV and vice versa. Thus, they have cautioned that a CME may undergo genuine acceleration even in the HI FOV, which extends from 15 to 84 $R_\odot$ for HI-1 and from 66 to 318 $R_\odot$ for HI-2.

Previous studies have reported that acceleration of a CME shows bimodal distribution (Chen & Krall 2003). We observe such a bimodal distribution in three CMEs, the ones which are not associated with prominence eruptions. The residual acceleration for the very impulsive 2007 December 31 CME was 90 m s^{-2}, while for the CMEs on 2007 November 16 and 2009 December 16, it was found to be 18 m s^{-2} and -2 m s^{-2}, respectively. The other CMEs, which are associated with prominences, do not show such an acceleration profile. Chen & Krall (2003) have invoked the flux injection mechanism to trigger an eruption in a magnetic flux rope, which leads to the residual acceleration phase. In the cases analyzed here, we observe that only the flare-associated CMEs undergo residual acceleration, which indicates that flux injection seems to be a good explanation for eruption of the flare-associated CMEs studied here, but a different mechanism should be considered for EP-associated CMEs.

Of the three CMEs associated with prominences, the 2010 April 13 and 2010 August 1 CMEs were associated with large quiescent polar crown prominences, while the one on 2008 April 9 was associated with an AR prominence. We find that the prominences on 2008 April 9 and 2010 April 13 showed a strong positive acceleration in the COR1 FOV, when their heights were close to almost 4 $R_\odot$. During the same time, however, acceleration of the CME LE was decreasing. This indicates that

even at a height of 4 $R_\odot$, forces acting on the CME and the EP cannot be considered the same, as suggested by Srivastava et al. (2000) and Maričić et al. (2004).

Thus, in this study, from the 3D reconstruction of six CMEs and EPs associated with three of them, we have observed some aspects of their acceleration, as detailed above, which were not previously reported. We find that the maximum CME acceleration occurs at a height of less than 2 $R_\odot$, where earlier this height was believed to be between 2–4 $R_\odot$. The bimodal acceleration profile was not observed in EP-associated CMEs, but in only those CMEs that were not associated with EPs. Two of the three prominences in the study showed a high and increasing value of acceleration at a distance of almost 4 $R_\odot$ but the corresponding CME LE does not show the same behavior. The CME on 2007 December 31 showed acceleration of over 1500 m s^{-2}, which is unusually high for a CME associated with a C-class flare.

The authors thank the *STEREO*/SECCHI consortium for providing the data. The SECCHI data used here were produced by an international consortium of the Naval Research Laboratory (USA), Lockheed Martin Solar and Astrophysics Lab (USA), NASA Goddard Space Flight Center (USA), Rutherford Appleton Laboratory (UK), University of Birmingham (UK), Max-Planck-Institut for Solar System Research (Germany), Centre Spatiale de Liège (Belgium), Institut d'Optique Theorique et Appliquée (France), and Institut d'Astrophysique Spatiale (France). Work by N.S. partially contributes to the research on collaborative NSF grant ATM-0837915 to Helio Research.

REFERENCES

Alexander, D. 2006, Space Sci. Rev., 123, 81
Alexander, D., Metcalf, T. R., & Nitta, N. V. 2002, Geophys. Res. Lett., 29, 1403
Brueckner, G. E., Howard, R. A., Koomen, M. J., et al. 1995, Sol. Phys., 162, 357
Cargill, P. J. 2004, Sol. Phys., 221, 135
Chen, J. 1989, ApJ, 338, 453
Chen, J., & Krall, J. 2003, J. Geophys. Res., 108, 1410
Chen, J., Marqué, C., Vourlidas, A., Krall, J., & Schuck, P. W. 2006, ApJ, 649, 452
Davis, C. J., Kennedy, J., & Davies, J. A. 2010, Sol. Phys., 263, 209
Domingo, V., Fleck, B., & Poland, A. I. 1995, Space Sci. Rev., 72, 81
Forbes, T. G. 2000, J. Geophys. Res., 105, 23153
Forbes, T. G., Linker, J. A., Chen, J., et al. 2006, Space Sci. Rev., 123, 251
Gopalswamy, N., Lara, A., Lepping, R. P., et al. 2000, Geophys. Res. Lett., 27, 145
Gopalswamy, N., Lara, A., Yashiro, S., Kaiser, M. L., & Howard, R. A. 2001, J. Geophys. Res., 106, 29207
Gosling, J. T., Hildner, E., MacQueen, R. M., et al. 1976, Sol. Phys., 48, 389
Howard, R. A., Moses, J. D., Vourlidas, A., et al. 2008, Space Sci. Rev., 136, 67
Joshi, A. D., & Srivastava, N. 2011, ApJ, 730, 104
Kaiser, M. L., Kucera, T. A., Davila, J. M., et al. 2008, Space Sci. Rev., 136, 5
Klimchuk, J. A. 2001, in Space Weather, ed. P. Song, H. Singer, & G. Siscoe (Geophysical Monograph 125; Washington, DC: AGU), 143
Krall, J., Chen, J., & Santoro, R. 2000, ApJ, 539, 964
Lin, C., Gallagher, P. T., & Raftery, C. L. 2010, A&A, 516, A44
Low, B. C. 2001, J. Geophys. Res., 106, 25141
MacQueen, R. M., & Fisher, R. R. 1983, Sol. Phys., 89, 89
Manoharan, P. K., & Mujiber Rahman, A. 2011, J. Atmos. Sol.-Terr. Phys., 73, 671
Maričić, D., Vršnak, B., Stanger, A. L., & Veronig, A. 2004, Sol. Phys., 225, 337
Maričić, D., Vršnak, B., Stanger, A. L., et al. 2007, Sol. Phys., 241, 99
Mierla, M., Inhester, B., Antunes, A., et al. 2010, Ann. Geophys., 28, 203
Moon, Y.-J., Choe, G. S., Wang, H., et al. 2002, ApJ, 581, 694
Neupert, W. M., Thompson, B. J., Gurman, J. B., & Plunkett, S. P. 2001, J. Geophys. Res., 106, 25215
Priest, E. R. 1988, ApJ, 328, 848
Raftery, C. L., Gallagher, P. T., McAteer, R. T. J., Lin, C., & Delahunt, G. 2010, ApJ, 721, 1579
Seaton, D. B., Mierla, M., Berghmans, D., Zhukov, A. N., & Dolla, L. 2011, ApJ, 727, L10
Shanmugaraju, A., Moon, Y.-J., Dryer, M., & Umapathy, S. 2003, Sol. Phys., 215, 185
Sheeley, N. R., Walters, J. H., Wang, Y.-M., & Howard, R. A. 1999, J. Geophys. Res., 104, 24739
Srivastava, N., Schwenn, R., Inhester, B., Martin, S. F., & Hanaoka, Y. 2000, ApJ, 534, 468
Srivastava, N., Schwenn, R., Inhester, B., Stenborg, G., & Podlipnik, B. 1999, Space Sci. Rev., 87, 303
Temmer, M., Veronig, A. M., Kontar, E. P., Krucker, S., & Vršnak, B. 2010, ApJ, 712, 1410
Thernisien, A., Vourlidas, A., & Howard, R. A. 2009, Sol. Phys., 256, 111
Thernisien, A. F. R., Howard, R. A., & Vourlidas, A. 2006, ApJ, 652, 763
Vršnak, B. 2001, J. Geophys. Res., 106, 25249
Vršnak, B., Žic, T., Falkenberg, T. V., et al. 2010, A&A, 512, A43
Yashiro, S., Gopalswamy, N., Michalek, G., et al. 2004, J. Geophys. Res., 109, 7105
Zhang, J., & Dere, K. P. 2006, ApJ, 649, 1100
Zhang, J., Dere, K. P., Howard, R. A., Kundu, M. R., & White, S. M. 2001, ApJ, 559, 452